American Journal of Mechanical Engineering, 2019, Vol. 7, No. 4, 158-171
Available online at http://pubs.sciepub.com/ajme/7/4/2
Published by Science and Education Publishing
DOI:10.12691/ajme-7-4-2

Modeling and Control Approach for a Complex-Shaped Underwater Vehicle

G.A.C.T. Bandara*, D.A.A.C. Ratnaweera, D.H.S. Maithripala

Department of Mechanical Engineering, University of Peradeniya, KY 20400, Sri Lanka
*Corresponding author: chanakatb@eng.pdn.ac.lk

Received August 19, 2019; Revised September 26, 2019; Accepted October 16, 2019

Abstract This paper presents the trajectory tracking and the path planning algorithm based on an adaptive control law to operate a complex-shaped low speed autonomous underwater vehicle (AUV) in a challenging environment of non-linearity, time variance and unpredictable external disturbances. Firstly, computational fluid dynamic (CFD) simulations are used to compute the added mass matrix and the damping matrix. Secondly, the adaptive controller is implemented to track the desired trajectory. This desired state-dependent regressor matrix-based controller provides consistent results even under hydrodynamic parametric uncertainties. The stability of the developed controller is verified using Lyapunov's direct approach. Moreover, the proposed control law adopts quaternions to represent the attitude errors and thus avoids the representation of singularities that occur when using the Euler angle description of the orientation. Thirdly, an efficient underwater path planning algorithm is developed based on vehicle-fixed-frame error variables. The simulations are done to compute the optimal path of the AUV which minimizes the travelling time. Finally, an optimal thrust allocation for the desired values of forces and moments acting on the vehicle is found via a model-based unconstrained thrust allocation. The results show that the AUV asymptotically converges on the desired trajectory and the path with a minimum time. At this moment, the propulsion forces approach zero, which further assures the accuracy of the controller. Hence, the effectiveness and the robustness of the developed algorithm are acceptable to design the AUV.

Keywords: *autonomous underwater vehicle (AUV), CFD modelling, adaptive control, trajectory, path planning, optimal thrust allocation*

Cite This Article: G.A.C.T. Bandara, D.A.A.C. Ratnaweera, and D.H.S. Maithripala, "Modeling and Control Approach for a Complex-Shaped Underwater Vehicle." *American Journal of Mechanical Engineering*, vol. 7, no. 4 (2019): 158-171. doi: 10.12691/ajme-7-4-2.

1. Introduction

Over last two decades, autonomous underwater vehicles (AUVs) have played major roles in underwater applications, and have a large variety of types and shapes. Especially small size, complex-shaped AUVs have more flexibility to reach the areas where remote operating vehicles (ROVs) and human occupied vehicles (HOVs) cannot be deployed. AUVs can also be operated in risky and hazardous environments. Meanwhile, complex-shaped AUVs have more DOFs than conventional torpedo-shaped AUVs to increase the maneuverability in complex underwater spaces.

There are three key factors to be considered in the motion control of an AUV: First, an accurate hydrodynamic model, second, an advanced control system, and third, an optimum thrust allocation. Yamamoto revealed in [1] that a model-based control system is more effective in case of dynamics of the AUV is known to some extent. Furthermore, an empirical model generally fails to represent the dynamics of the AUV over a wide operating region that was noticed by Ferreira [2]. Thus, to get an accurate hydrodynamic model of the complex-shaped AUVs is vital to design a controller. In addition to that, it is an arduous task to build a suitable controller for an AUV due to the complexity of hydrodynamic parameters containing highly non-linear and coupled terms. Moreover, the literature in the field of the optimum thrust allocation is little to be known [3]. Particularly, the importance of the optimization of the thrust forces of AUVs has been disregarded so far.

Scaled and full-scaled experiment, empirical formula, and computational approach are the existing methods to model the underwater vehicles. The scaled and full-scaled experiments are the most expensive methods because these ones require costly devices like towing tanks, but provide accurate hydrodynamic parameters. References [4,5] provide the methods to do the experiments without the towing tank. Furthermore, the empirical formulas usually give the acceptable results on the underwater vehicles that have slender bodies such as torpedo-shaped AUVs as noticed in [6]. Lastly, computation approaches are the best way to find the hydrodynamic parameters under low cost. Nevertheless, vast knowledge and experience are the prime factors to model the complex-shaped AUVs. Potential and finite element theory-based software such as

ANSYS FLUENT™, ANSYS AQWA™, ANSYS CFX™, and WAMIT™ is used in this method. WAMIT™ overcomes the other software to compute the added mass matrix [7]. Similarly, ANSYS CFX™ leads the case of finding damping matrix [8].

There are so many control systems proposed to the track trajectories and to plan the desired path for AUVs. The horizontal tracking control for the AUVs based on a non-linear sliding mode incremental feedback model was introduced in [9] to track the desired trajectories. The error dynamics on the horizontal plane were proposed in [10] to plan and track the trajectories using the closed loop tracking controller and the backstepping method was used to stabilize the system. To track the given trajectories in the presence of ocean currents, a feedback controller was introduced in [11] using ling of sight (LOS), and a sliding mode controller based on both LOS and cross track error approach was presented in [12]. The trajectory planning for the AUVs was addressed in [13] to provide ocean processes of the real-time ocean model. The wheel robot was controlled to track the desired trajectories in [14] using a linearized fuzzy adaptive controller with the backstepping feedback. The trajectory tracking of the AUVs was implemented using the adaptive tracking controller based on a radial basis function neural network (RBF-NN) [15]. A dynamic surface control (DSC) and minimal learning parameters (MLP) based on a robust adaptive neural network tracking control for the underwater vehicle have been used in [16]. The learning method of a neural network has been used to model the stability and robustness adaptive controller for a nonholonomic robot [17]. In [18,19], they have described the path planning method based on a velocity field using the starting point and the desired ending point within a minimum time period. The coordinate path followed by underactuated AUVs was outlined, based on the convergence of geometric errors with respect to the origin of the vehicle that coincides with the center of gravity [20]. The path tracking based on the marching algorithm has been used in [21] for the path planning on a fixed depth. The combined path following and trajectory tracking for the AUVs have been discussed in [22] using the backstepping method, where Lyapunov's direct approach was used to develop the kinematic of the AUVs. The optimal path planning for the AUVs in fast flowing, complex fluid flow was proposed using the methods of cost function, parametrization, and principle of minimum energy [19].

Recommended techniques of finding the hydrodynamic, trajectory tracking and path planning methods for AUVs have been noted in literature. However, an uncertainty of their hydrodynamic parameters, including non-linear hydrodynamic effects, parameter variations, and ocean current disturbance, causes difficulties when designing the suitable controllers. To overcome these problems, there should be a controller that could be operated under the well-defined hydrodynamic model.

In our work, the complex-shaped AUV that was used for the simulations is shown in Figure 1. The placement of 6 thrusters is only considered in Section 5. Furthermore, the configuration details of the AUV are listed in Table 1.

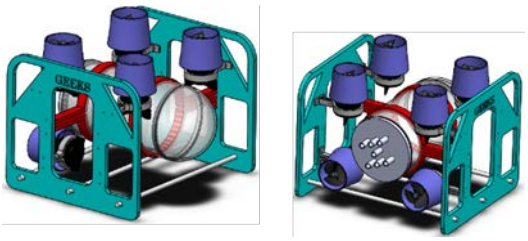

Figure 1. 3D CAD images of the AUV [23]

Table 1. Characteristics of the complex-shaped AUV

Size	(L) 0.525 m, (W) 0.406 m, (H) 0.395 m
Weight in air	16.00 kg
Propulsion	2 Horizontal and 4 vertical propellers
Degrees of freedom	Surge, Sway, Heave, Roll, Pitch, Yaw
Speed	$0 - 0.6\ m/s$

This paper presents a modelling and adaptive controlling approach for the complex-shaped AUV. In Section 2, the standard notions for marine vehicles are introduced. Section 3 is focused to develop the model of the complex-shaped AUV to find the hydrodynamic parameters using the computational approach, ANSYS FLUENT™. In Section 4, the vehicle-fixed frame adaptive controller is introduced to track the desired trajectories under the presence of hydrodynamic uncertainties, and uses the quaternion-based attitude error. Finally, the path planning method is developed based on the trajectory tracking controller, and the approach to find the minimum thrust allocation is proposed to increase the effectiveness of the propulsion system in Section 5. To the best of our knowledge, this is the first time that the representation of the quaternion-based attitude error is used for the trajectory tracking and path planning with a complete hydrodynamic analysis.

2. AUV Modeling

This section is committed to represent the AUV kinematics and dynamics containing highly non-linear and coupled terms which make the mathematical model challengeable. NED-frame (North East Down) and B-frame (Body fixed frame) are the two coordinate frames for marine systems introduced for convenience by Fossen in [24] and shown in Figure 2.

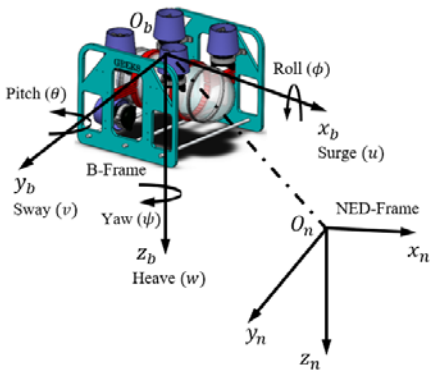

Figure 2. NED frame and B-frame of underwater vehicles

The AUV dynamics are based on the marine vehicle formulation by Fossen in [24] and [25], and by the Society of Naval Architects and Marine Engineers (SNAME) [26]. Positions, angles, linear and angular velocities, force and moment are shown in Table 2. The position vector (η), velocity vector (υ), and force vector (τ) are defined as follows.

$$\eta = [x, y, z, \phi, \theta, \psi]^{\mathrm{T}} \tag{1}$$

$$v = [u, v, w, p, q, r]^{\mathrm{T}} \tag{2}$$

$$\tau = [X, Y, Z, K, M, N]^{\mathrm{T}}. \tag{3}$$

Table 2. The notation of SNAME for marine vessels

	Position and Angles (η)		Linear and Angular Velocities (v)		Forces and moments (τ)
Co-ordinate	NED- frame		B-frame		B-frame
Surge	x	η_1	u	v_1	X
Sway	y		v		Y
Heave	z		w		Z
Roll	ϕ	η_2	p	v_2	K
Pitch	θ		q		M
Yaw	ψ		r		N

The dynamic equation of motion is given by

$$M\dot{v} + C(v)v + D(v)v + g(\eta) = \tau + \tau^{e}. \tag{4}$$

Rigid body mass-inertia matrix (M_{RB}) defined in (5). m is the mass of the AUV and $r_G = [x_G, y_G, z_G]^T$ is the position vector from the origin of the body frame O_b to the Center of Gravity (COG). In this case, the origin of the body-fixed frame is coincided with the COG of the AUV. Then, the mass-inertia matrix is extremely reduced. It is assumed that the AUV is symmetric about $x_b = 0$ and $y_b = 0$ planes. Therefore, the inertia components become roughly diagonal form

$$M_{RB} = \begin{bmatrix} m & 0 & 0 & 0 & mz_G & -my_G \\ 0 & m & 0 & -mz_G & 0 & mx_G \\ 0 & 0 & m & my_G & -mx_G & 0 \\ 0 & -mz_G & my_G & I_{xx} & -I_{xy} & -I_{xz} \\ mz_G & 0 & -mx_G & -I_{yx} & I_{yy} & -I_{yz} \\ -my_G & mx_G & 0 & -I_{zx} & -I_{zy} & I_{zz} \end{bmatrix}. \tag{5}$$

Let M_A be the added mass and inertia.

$$M_A = \begin{bmatrix} X_{\dot{u}} & X_{\dot{v}} & X_{\dot{w}} & X_{\dot{p}} & X_{\dot{q}} & X_{\dot{r}} \\ Y_{\dot{u}} & Y_{\dot{v}} & Y_{\dot{w}} & Y_{\dot{p}} & Y_{\dot{q}} & Y_{\dot{r}} \\ Z_{\dot{u}} & Z_{\dot{v}} & Z_{\dot{w}} & Z_{\dot{p}} & Z_{\dot{q}} & Z_{\dot{r}} \\ K_{\dot{u}} & K_{\dot{v}} & K_{\dot{w}} & K_{\dot{p}} & K_{\dot{q}} & K_{\dot{r}} \\ M_{\dot{u}} & M_{\dot{v}} & M_{\dot{w}} & M_{\dot{p}} & M_{\dot{q}} & M_{\dot{r}} \\ N_{\dot{u}} & N_{\dot{v}} & N_{\dot{w}} & N_{\dot{p}} & N_{\dot{q}} & N_{\dot{r}} \end{bmatrix} \tag{6}$$

where the conversation of SNAME is used; $X_{\dot{u}} = \dfrac{\partial X}{\partial \dot{u}}$, etc.

The rigid body induced Coriolis-centripetal matrix, and the added mass induced Coriolis-centripetal matrix are given by C_{RB} and C_A respectively. In our case, C_A matrix is neglected due to the slow speed of the AUV.

$$C_{RB}(v) = \begin{bmatrix} 0 & 0 & 0 & 0 & mw & -mv \\ 0 & 0 & 0 & -mw & 0 & mu \\ 0 & 0 & 0 & mv & -mu & 0 \\ 0 & mw & -mv & 0 & I_{zz}r & -I_{yy}q \\ -mw & 0 & mu & -I_{zz}r & 0 & I_{xx}p \\ mv & -mu & 0 & I_{yy}q & -I_{xx}p & 0 \end{bmatrix} \tag{7}$$

$$C_A(v) = \begin{bmatrix} 0 & 0 & 0 & 0 & -\alpha_3(v) & \alpha_2(v) \\ 0 & 0 & 0 & \alpha_3(v) & 0 & -\alpha_1(v) \\ 0 & 0 & 0 & -\alpha_2(v) & \alpha_1(v) & 0 \\ 0 & -\alpha_3(v) & \alpha_2(v) & 0 & -\beta_3(v) & \beta_2(v) \\ \alpha_3(v) & 0 & -\alpha_1(v) & \beta_3(v) & 0 & -\beta_1(v) \\ -\alpha_2(v) & \alpha_1(v) & 0 & -\beta_2(v) & \beta_1(v) & 0 \end{bmatrix} \tag{8}$$

where $\alpha_1(v) = X_{\dot{u}}u + Y_{\dot{v}}v + X_{\dot{w}}w + X_{\dot{p}}p + X_{\dot{q}}q + X_{\dot{r}}r$, $\alpha_2(v) = X_{\dot{v}}u + Y_{\dot{v}}v + Y_{\dot{w}}w + Y_{\dot{p}}p + Y_{\dot{q}}q + Y_{\dot{r}}r$, $\alpha_3(v) = X_{\dot{w}}u + Y_{\dot{w}}v + Z_{\dot{w}}w + Z_{\dot{p}}p + Z_{\dot{q}}q + Z_{\dot{r}}r$, $\beta_1(v) = X_{\dot{p}}u + Y_{\dot{p}}v + Z_{\dot{p}}w + K_{\dot{p}}p + K_{\dot{q}}q + K_{\dot{r}}r$, $\beta_2(v) = X_{\dot{q}}u + Y_{\dot{q}}v + Z_{\dot{q}}w + K_{\dot{q}}p + M_{\dot{q}}q + M_{\dot{r}}r$, and $\beta_3(v) = X_{\dot{r}}u + Y_{\dot{r}}v + Z_{\dot{r}}w + K_{\dot{r}}p + M_{\dot{r}}q + N_{\dot{r}}r$, also here the SNAME notion is used.

$D(v)v$ denotes the total hydrodynamic damping matrix. The hydrodynamic damping of the underwater vehicles normally contains four types of damping forces as below:

$$D(v) = D_l(v) + D_q(v) + D_p(v) + D_d(v) \tag{9}$$

where $D_l(v)$, $D_q(v), D_p(v)$, and $D_q(v)$ are the linear, quadratic, potential, and wave drift term respectively.

If the vehicle is symmetric about all the planes, then $D_l(v)$ becomes a diagonal matrix describing in [27] as follows:

$$D_l(v) = \begin{bmatrix} X_u & 0 & 0 & 0 & 0 & 0 \\ 0 & Y_v & 0 & 0 & 0 & 0 \\ 0 & 0 & Z_w & 0 & 0 & 0 \\ 0 & 0 & 0 & K_p & 0 & 0 \\ 0 & 0 & 0 & 0 & M_q & 0 \\ 0 & 0 & 0 & 0 & 0 & N_r \end{bmatrix}. \tag{10}$$

The axial quadratic drag force of the AUV can be model with

$$X = -\left(\frac{1}{2}\rho C_d A_f\right)u|u| = X_{u|u|}u|u| \tag{11}$$

where ρ is the fluid density; A_f is the cross-sectional area and C_d is the damping coefficient; $X_{u|u|} = \dfrac{\partial X}{\partial u|u|} = \dfrac{1}{2}\rho C_d A_f$.

The notion of (11) gives the quadratic drag matrix as shown below:

$$D_q(v) = \begin{bmatrix} X_{u|u|}|u| & 0 & 0 & 0 & 0 & 0 \\ 0 & Y_{v|v|}|v| & 0 & 0 & 0 & 0 \\ 0 & 0 & Z_{w|w|}|w| & 0 & 0 & 0 \\ 0 & 0 & 0 & K_{p|p|}|p| & 0 & 0 \\ 0 & 0 & 0 & 0 & M_{q|q|}|q| & 0 \\ 0 & 0 & 0 & 0 & 0 & N_{r|r|}|r| \end{bmatrix} \tag{12}$$

It is considered that the weight (W) of the AUV is approximately equal to the buoyance force (B). $g(\eta)$ is the gravitational and buoyance matrix. It can be simplified as in (13) as pointed out by [24]. $r_B = [x_B,\ y_B,\ z_B]^T$ is the position vector for the COG to the Center of Buoyancy (COB).

$$g(v) = \begin{bmatrix} (W-B)\sin(\theta) \\ -(W-B)\cos(\theta)\sin(\phi) \\ -(W-B)\cos(\theta)\cos(\phi) \\ \begin{pmatrix} -(y_G W - y_B B)\cos(\theta)\cos(\phi) \\ +(z_G W - z_B B)\cos(\theta)\sin(\phi) \end{pmatrix} \\ (z_G W - z_B B)\sin(\theta) + (x_G W - x_B B)\cos(\theta)\cos(\phi) \\ \begin{pmatrix} -(x_G W - x_B B)\cos(\theta)\sin(\phi) \\ -(y_G W - y_B B)\sin(\theta) \end{pmatrix} \end{bmatrix}. \quad (13)$$

τ is the forces and moments vector of the propulsion input, and the environmental forces and moments are defined as τ^e

The kinematic equation of the AUV can be expressed as

$$v = J_e\left(R_B^I\right)\dot{\eta} \quad (14)$$

where $J_e(R_B^I)$ is the velocity transformation matrix between the body-fixed frame of the AUV and the earth-fixed frame and R_B^I is the rotation matrix expressing the transformation from the earth-fixed frame to the body-fixed frame. This velocity transformation matrix is further represented as below.

$$J_e\left(R_B^I\right) = \begin{bmatrix} R_I^B & 0_{3\times3} \\ 0_{3\times3} & J_{k,o} \end{bmatrix} \quad (15)$$

where

$$R_I^B(\eta_2) = \begin{bmatrix} c\psi c\theta & s\psi c\theta & -s\theta \\ -s\psi c\phi + c\psi s\theta s\phi & c\psi c\phi + s\psi s\theta s\phi & s\phi c\theta \\ s\psi s\phi + c\psi s\theta c\phi & -c\psi s\phi + s\psi s\theta c\phi & c\phi c\theta \end{bmatrix},$$

$$J_{k,o}(\eta_2) = \begin{bmatrix} 1 & 0 & -s\theta \\ 0 & c\phi & s\phi c\theta \\ 0 & -s\phi & c\phi c\theta \end{bmatrix}$$

and $c\alpha$ and $s\alpha$ are the short notations for $\cos(\alpha)$ and $\sin(\alpha)$, respectively.

To overcome the possible occurrence of representation singularities, it might be convenient to resort to the quaternion representation ($Q = \{\varepsilon, \mu\}$). The relationship between v, η_1 and the time derivative of the quaternion $\dot{Q}$ is given by the quaternion propagation equations. (See Appendix A)

3. Computational Solutions for Dynamic and Hydrodynamic Parameters

This section represents how the numerical methods are used to find the rigid body mass-inertia matrix, added mass matrix, and damping matrix. First, the SOLIDWORKS software is used to compute the mass-inertia matrix (M_{RB}). Next, ANSYS FLUENT™ is used to find both added mass (M_A) and damping matrix ($D(V)$).

3.1. Rigid Body Mass Inertia Matrix

The COG and the inertia parameters of the AUV are very difficult to calculate analytically as shown in (16) in [24] because they have many different density components. The mass and inertia of a small particle can be defined as follow.

$$m = \int_0^V \rho_m dV,\ I = \int_0^V r^2 \rho_m dV \quad (16)$$

where ρ_m is the density of an element of volume dv. V is the total volume of the AUV, r is the distance between the element of volume dv and the COG.

The best way to calculate the mass-inertia matrix (M_{RB}) of the AUV is to use the CAD software, SOLIDWORKS. The SOLIDWORKS' model of the AUV is shown in Figure 1 and M_{RB} is listed in (17). Floating and payloads are not examined here. It is acceptable to neglect the off-diagonal inertia elements compared with the diagonal terms, expressed as follows. The units are measured in kg and kgm^2.

$$M_{RB} = \begin{bmatrix} 16.247 & 0 & 0 & 0 & 0 & 0 \\ 0 & 16.247 & 0 & 0 & 0 & 0 \\ 0 & 0 & 16.247 & 0 & 0 & 0 \\ 0 & 0 & 0 & 0.2568 & 0 & 0 \\ 0 & 0 & 0 & 0 & 0.3841 & 0 \\ 0 & 0 & 0 & 0 & 0 & 0.3716 \end{bmatrix}. \quad (17)$$

3.2. Added Mass Matrix

The added mass of the AUV really depends on the geometry of the underwater vehicle as mentioned in [28]. Hence, the use of empirical formulas predicting M_A and a hull approximation by elementary shapes are inaccurate for the complex-shaped AUV. For the case of a complex-shaped AUV, M_A matrix cannot pursue the empirical formulas noted in [5] and [6]. ANSYS FLUENT™ is advanced to compute the hydrodynamic characteristics of marine objects, offering the function to figure out the added mass matrix, and it requires a closed geometry of the AUV for the calculation. In this case, the speed of the AUV is low enough to neglect the off-diagonal elements. Thus, the diagonalized matrix is considered for the MATLAB simulations done in Section 4 and Section 5. The units are measured in kg and kgm^2.

$$M_A = \begin{bmatrix} 12.713 & -0.103 & -0.115 & 0.042 & 0.318 & 0.017 \\ 0.158 & 21.827 & -0.156 & 0.087 & -0.019 & -0.785 \\ 0.138 & -0.151 & 69.689 & -0.039 & 0.723 & 0.072 \\ 0.143 & 0.405 & -0.063 & 0.524 & 0.004 & -0.016 \\ 0.507 & -0.004 & 0.742 & -0.005 & 0.971 & 0.004 \\ -0.008 & -0.796 & 0.082 & -0.006 & 0.006 & 0.212 \end{bmatrix} \quad (18)$$

3.3. Damping Matrix

In this case, $D_p(v)$ can be neglected comparing to other terms, and $D_d(v)$ is also ignored since the AUV operates under certain depth, shown in [24].

These formulas are impractical to calculate the damping matrix. Hence, ANSYS FLUENT™ based on the finite element theory is used to compute the relationship between the damping forces and velocity of the AUV. The AUV is fixed in a rectangular tank in which the velocity of the fluid varies from 0 to 0.6 m/s (approximation of general AUV operating speed), with the speed interval of 0.1 m/s.

The velocity stream-line views of ANSYS FLUENT™ results in different directions are shown in Figure 3. The configuration details used for the simulation are listed in Table 3, and the computed damping forces and moments are listed in Table 4 and Table 5. A second order polynomial relationship is noticed between damping forces/moments and velocities, see Figure 4 and Figure 5.

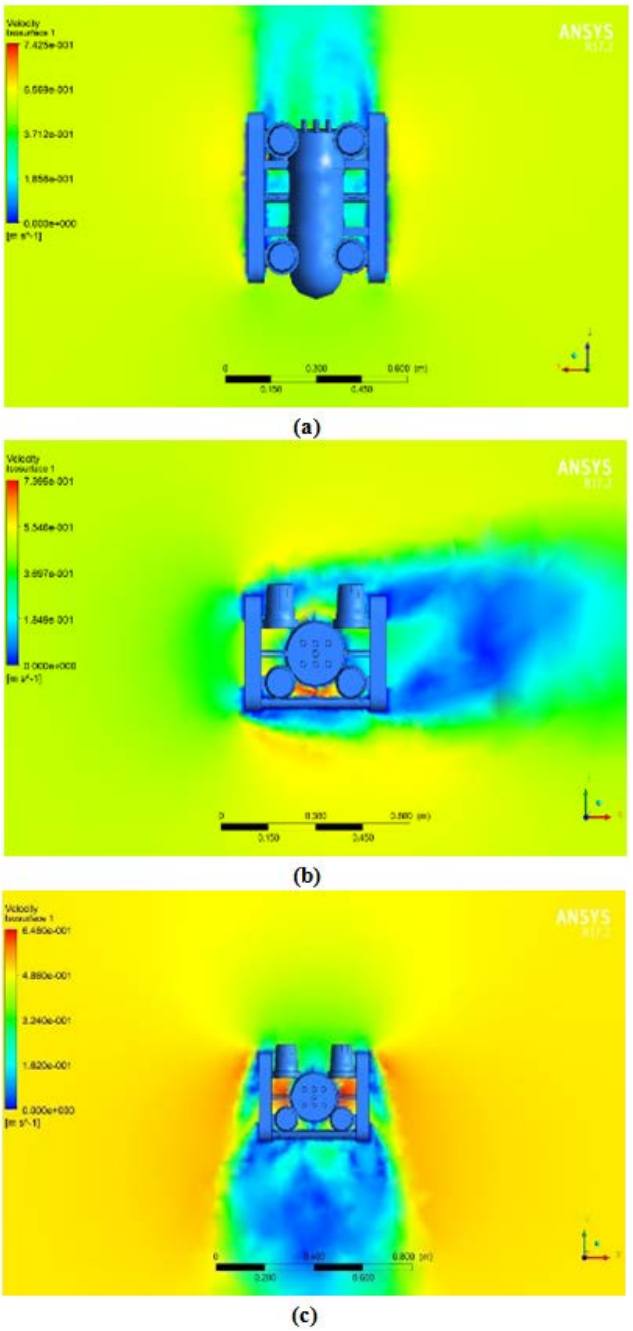

Figure 3. ANSYS FLUENT™ velocity streamline views of the AUV at 0.5 m/s: (a) in surge direction; (b) in sway direction; (c) in heave direction

Table 3. Configuration details of ANSYS FLUENT™

Parameter	Description
Tank	$12m$ (L) $5m$ (W) $5m$ (H)
Fluid	Sea water. Viscosity= $1.60 \times 10^{-6}\ kg/(sm)$ at 5℃ and salinity 4%, density = 1023 kg/m^3
Turbulence	Sheer stress transport 1% at inlet boundary
Mesh size	596455 elements
Convergence	6×10^{-5}
Roughness	$0.0015 - 0.009\ mm$

Table 4. Damping forces at different linear velocities

Linear velocity/(m/s)	0.1	0.2	0.3	0.4	0.5	0.6
Surge/(N)	0.322	1.287	2.893	5.141	8.032	11.564
Sway/(N)	0.563	2.253	5.069	9.013	14.080	20.275
Heave/(N)	0.736	2.943	6.622	11.773	18.395	26.488

Table 5. Damping torques at different angular velocities

Angular velocity/(rad/s)	0.5	1	1.5	2	2.5	3
Roll/(Nm)	0.120	0.387	0.800	1.360	2.066	2.919
Pitch/(Nm)	0.319	0.904	1.754	2.870	4.251	5.898
Yaw/(Nm)	0.149	0.470	0.964	1.630	2.469	3.480

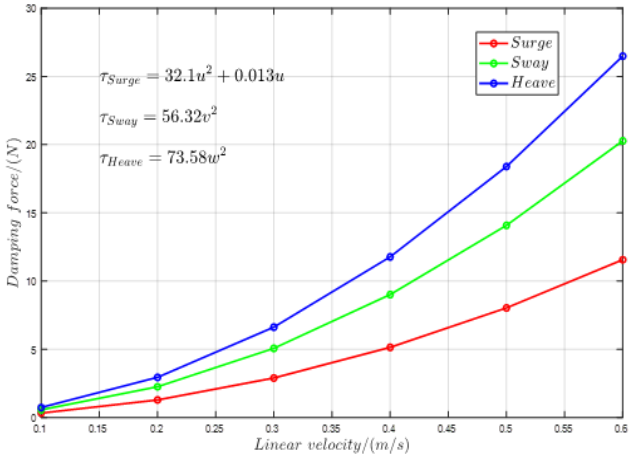

Figure 4. Estimated damping force with linear velocity

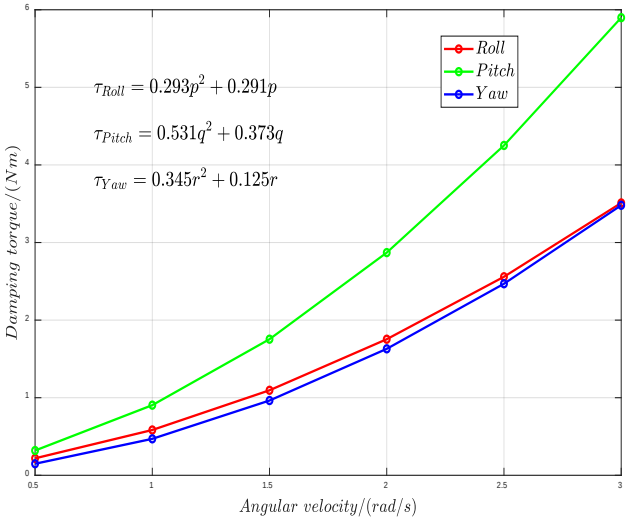

Figure 5. Estimated damping torque with angular velocity

4. Trajectory Tracking Control Law

The dynamics of the AUV denoted in (4) include the uncertainty of the parameters in the damping matrix. It is designed to recompense the uncertainties; therefore, the vehicle-fixed-frame adaptive controller is proposed to achieve a consistent AUV performance by estimating uncertain parameters. The parameters in the control law are adjusted by an adaption mechanism. The proposed adaptive controller is designed to force the AUV to follow the desired trajectory with the existence of a parameter uncertainty. For this, a regression matrix should be defined.

Let us consider the vehicle-fixed variables

$$\tilde{y}=\begin{bmatrix} R_I^B\tilde{\eta}_1 \\ \tilde{\varepsilon} \end{bmatrix} \tag{19}$$

$$\tilde{v}=v_d-v \tag{20}$$

where $\tilde{\eta}_1=\eta_1-\eta_{1,d}$ being $\eta_{1,d}$ the desired position, and the quaternion-based attitude error is given by $\tilde{\varepsilon}$. v_d is the desired velocity of the AUV in the body-fixed frame.

The error vector is given by:

$$S=v+\Lambda y \tag{21}$$

with $\Lambda=$ positive definite matrix.

The vehicle regressor matrix

$$\Phi=\Phi\left(v,\dot{v},v_d,\dot{v}_d\right) \tag{22}$$

The adaptive control law can be defined in the following form.

$$\tau=\Phi\left(v,\dot{v},v_d,\dot{v}_d\right)\hat{\Theta}+K_DS. \tag{23}$$

Such that,

$$\begin{aligned} &M\dot{v}_d+C(v)v_d+D(v)v_d+g(\eta) \\ &=\Phi\left(v,\dot{v},v_d,\dot{v}_d\right)\hat{\Theta}+K_DS \end{aligned} \tag{24}$$

where K_D is a (6×6) positive definite matrix. The parameter estimate $\hat{\Theta}$ is updated by

$$\dot{\hat{\Theta}}=\Gamma\Phi^{\mathrm{T}}S \tag{25}$$

where Γ is a suitable positive definite matrix of an appropriate dimension, and is selected in such a way that the tuning law provides convergent characteristics.

The adaptive law proposed in the equation can drive the AUV in a desired manner, and guarantee the AUV's stability. The structure of the proposed control is given in the block diagram below.

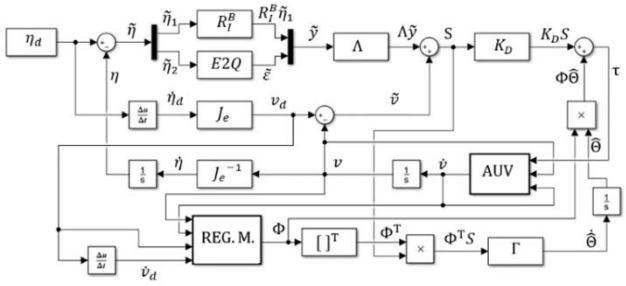

Figure 6. MATLAB SIMULINK layout of the proposed adaptive control law

4.1. Stability of the Proposed Control Law

The following Lyapunov candidate function is used to examine the stability of the system.

$$\begin{aligned} &V(t)=\frac{1}{2}\left[S^TMS+\tilde{\Theta}^{\mathrm{T}}\Gamma^{-1}\tilde{\Theta}\right]=V_1(t)+V_2(t), \\ &\tilde{\Theta}=\hat{\Theta}-\Theta,\forall S\neq 0,\tilde{\Theta}\neq 0 \end{aligned} \tag{26}$$

where $V_1(t)=\frac{1}{2}S^{\mathrm{T}}MS$ and $V_2(t)=\frac{1}{2}\tilde{\Theta}^{\mathrm{T}}\Gamma^{-1}\tilde{\Theta}$.

The selected Lyapunov candidate function satisfies the conditions given in (27).

$$\begin{aligned} &V(t):R^n\rightarrow R \text{ such that} \\ &V(t)\geq 0, \text{ if and only if } t=0\left(\text{positive definite}\right) \\ &\dot{V}(t)=\frac{dV(t)}{dt}\leq 0, \text{ if and only if } t=0\,(\text{negative definite}) \end{aligned} \tag{27}$$

Indeed, the system is asymptotically stable in the sense of Lyapunov because $V(t)$ satisfies the above conditions.

The time derivative of (26) is given by

$$\dot{V}(t)=\dot{V}_1(t)+\dot{V}_1(t) \tag{28}$$

Being $\dot{V}_1(t)$ and $\dot{V}_2(t)$ as follows,

$$\dot{V}_1(t)=S^{\mathrm{T}}M\dot{S}+\frac{1}{2}S^{\mathrm{T}}\dot{M} \tag{29}$$

$$\dot{V}_2(t)=\dot{\hat{\Theta}}^{\mathrm{T}}\Gamma^{-1}\tilde{\Theta} \tag{30}$$

where $\dot{\tilde{\Theta}}=\dot{\hat{\Theta}}+0$, as Θ is a constant definite vector

Substituting (21) into (29), as shown in [29].

$$\dot{V}_1(t)=S^{\mathrm{T}}M\left(\dot{v}_d-\dot{v}\right)+\frac{1}{2}S^{\mathrm{T}}\dot{M}S \tag{31}$$

where $S=v_d-v$

Substituting the value of $M\dot{v}$ from (4) into (31) and simplifying for $\dot{V}_1(t)$

$$\dot{V}_1(t)=S^{\mathrm{T}}\left(M\dot{v}_d+Cv+Dv+g-\tau\right)+\frac{1}{2}S^{\mathrm{T}}\dot{M}S \tag{32}$$

$$\dot{V}_1(t)=S^{\mathrm{T}}\begin{pmatrix} M\dot{v}_d+C\left(-s+v_d\right) \\ +D\left(-s+v_d\right)+g-\tau \end{pmatrix}+\frac{1}{2}S^{\mathrm{T}}\dot{M}S \tag{33}$$

$$\begin{aligned} \dot{V}_1(t)&=S^{\mathrm{T}}\left(M\dot{v}_d+Cv_d+Dv_d+g-\tau\right) \\ &+\frac{1}{2}S^{\mathrm{T}}\left(\left(\dot{M}-2(C+D)\right)S\right) \end{aligned} \tag{34}$$

$\dot{M}-2(C+D)$ is a skew-symmetric matrix for the AUVs. Substituting the system dynamics given in (4) into above equation.

$$\dot{V}_1(t)=S^{\mathrm{T}}\left(Y\Theta-\tau\right) \tag{35}$$

Therefore, equation (28) becomes,

$$\dot{V}(t)=S^{\mathrm{T}}\left(Y\hat{\Theta}-\tau\right)+\dot{\hat{\Theta}}^{\mathrm{T}}\Gamma^{-1}\tilde{\Theta} \tag{36}$$

Substituting the control input (τ) into (36)

$$\dot{V}(t)=S^{\mathrm{T}}\left(\Phi\Theta-\Phi\hat{\Theta}-K_DS\right)+\dot{\hat{\Theta}}^{\mathrm{T}}\Gamma^{-1}\tilde{\Theta} \tag{37}$$

$$\dot{V}(t) = S^{\mathrm{T}}\left(-\Phi\tilde{\Theta} - K_D S\right) + \hat{\Theta}^{\mathrm{T}}\Gamma^{-1}\tilde{\Theta} \quad (38)$$

$$\dot{V}(t) = -S^{\mathrm{T}}\Phi\tilde{\Theta} - S^{\mathrm{T}}K_D S + \hat{\Theta}^{\mathrm{T}}\Gamma^{-1}\tilde{\Theta}. \quad (39)$$

Substituting $\hat{\dot{\Theta}}$ from (25) into (39)

$$\dot{V}(t) = -S^{\mathrm{T}}\Phi\tilde{\Theta} - S^{\mathrm{T}}K_D S + (\Gamma\Phi^{\mathrm{T}}S)^{\mathrm{T}}\Gamma^{-1}\tilde{\Theta} \quad (40)$$

$$\dot{V}(t) = -S^{\mathrm{T}}K_D S \leq 0 \quad (41)$$

Equation (41) satisfies the Lyapunov stability criterion of the AUV dynamics with a stable controller. Therefore, the adaptive control law proposed in (23) gives a stable closed system.

4.2. Validation of the Adaptive Controller

The derivation of the regressor matrix of a high-DOF is very cumbersome. Therefore, for the sake of simplicity, only five DOFs are considered.

$$M\dot{v}_d + Dv_d = \tau \quad (42)$$

where

$$M = diag\left(m_{11} + m_{22} + m_{33} + m_{44} + m_{55}\right),$$

$$D = diag\left(d_{11} + d_{22} + d_{33} + d_{44} + d_{55}\right),$$

$v_d = [u_d, u_d, w_d, q_d, r_d]^{\mathrm{T}}$, and $\tau = \Phi\hat{\Theta} + K_D S$.

When the regression matrix Φ is used, the AUV model given in (42) can be written down in the form of linear parameters. For a real-time implementation, it is clear that the regression matrix, a state dependent matrix, is needed to calculate in each control cycle, seen in [30].

The regression matrix defined in (22) can be written as follows:

$$\Phi\left(v_d, \dot{v}_d\right) = \begin{bmatrix} \dot{u}_d & |u_d|u_d & 0 & 0 & 0 & 0 & 0 & 0 & 0 & 0 \\ 0 & 0 & \dot{v}_d & |v_d|v_d & 0 & 0 & 0 & 0 & 0 & 0 \\ 0 & 0 & 0 & 0 & \dot{w}_d & |w_d|w_d & 0 & 0 & 0 & 0 \\ 0 & 0 & 0 & 0 & 0 & 0 & \dot{q}_d & |q_d|q_d & 0 & 0 \\ 0 & 0 & 0 & 0 & 0 & 0 & 0 & 0 & \dot{r}_d & |r_d|r_d \end{bmatrix} \quad (43)$$

The number of simulations is performed with the desired trajectories to check the validity of the proposed control. The parameters of the AUV used for simulations are listed in Table 6.

The desired trajectory in the form of a circular path.

$$\begin{aligned} x_d &= 5\sin\left(0.02t\right), \\ y_d &= 5\cos\left(0.02t\right), z_d = 0.5\sin\left(0.02t\right), \\ \theta_d &= \frac{\pi}{4}, \psi_d = \frac{\pi}{6}, \end{aligned} \quad (44)$$

Note: The selected trajectory functions should be continuous to compute the second derivative with respect to time.

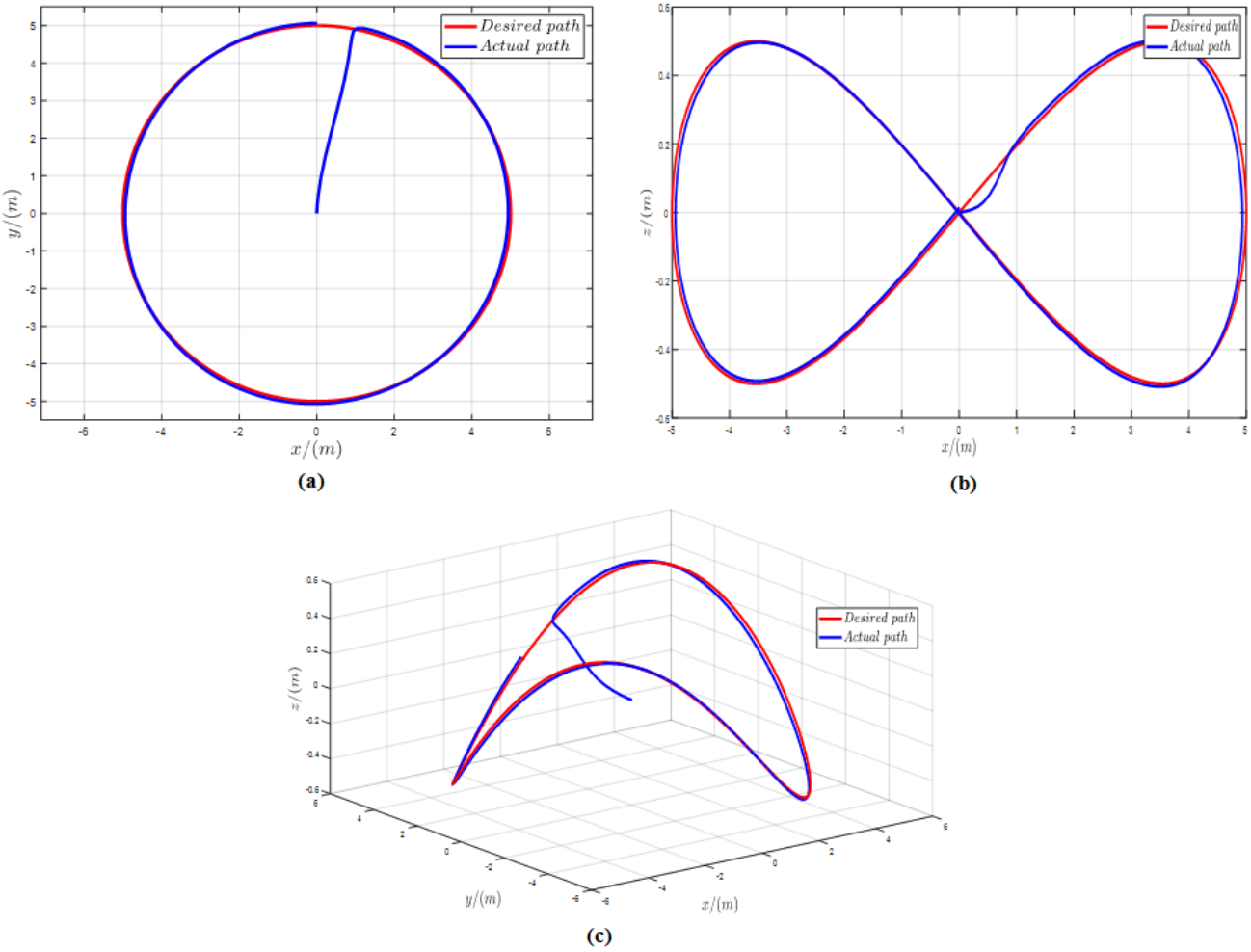

Figure 7. Circular trajectory comparison between the desired path and actual path projected onto: **(a)** xy plane; **(b)** xz plane and plotted; **(c)** in $\mathbb{R}^3$ space

Table 6. Parameters of the AUV used for the simulation

Mass/(kg, kgm^2)	Damping coefficient/$(kg/s\,, kgm^2/s)$	Gain matrix
m_{11}=28.960	$D_{11} = 32.1u^2 + 0.013\|u\|$	$K_D = diag([10, 15, 40, 10, 10])$
m_{22}=38.074	D_{22} = $56.32v^2$	$\Lambda = diag([45, 15, 20, 20, 20])$
m_{33}=85.936	D_{33} = $73.58w^2$	$\Gamma = diag([170, 15, 30, 20, 30, 20, 10, 10, 10, 10])$
m_{44}=1.355	D_{44} = $0.531q^2 + 0.373\|q\|$	
m_{55}=0.584	D_{55} = $0.345r^2 + 0.125\|r\|$	

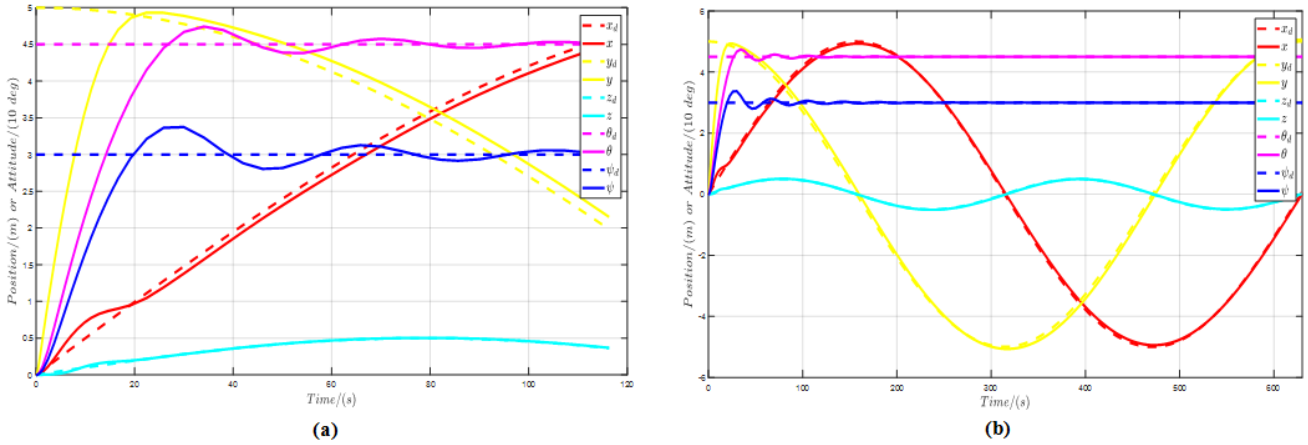

Figure 8. Actual position and attitude of the AUV compared with the desired position and attitude: (a) after 120 *s*; (b) after 630 *s*

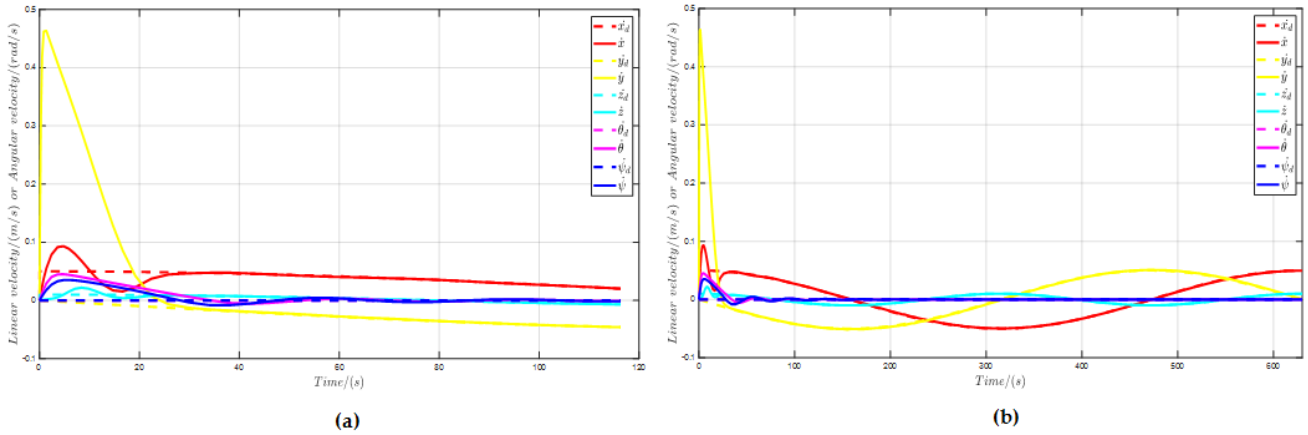

Figure 9. Earth-fixed linear and angular velocities: (a) after 120 *s*; (b) after 630 *s*

Figure 8 elaborates that the actual position and orientation of the AUV accurately track the desired position and orientation after 95 *s*.

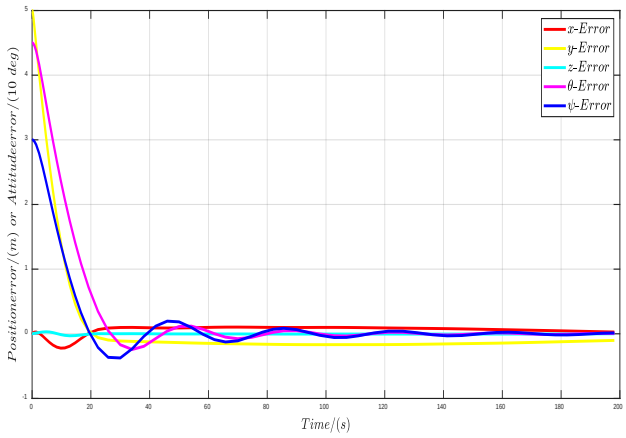

Figure 10. Position and attitude errors of the AUV after 200 *s*

Figure 9 illustrates that the velocity errors tended to zero within 85 *s* from the beginning. And also, Figure 10 and Figure 11 asymptotically converge to zero. Thus, the proposed controller accurately commands the AUV to follow the desired path.

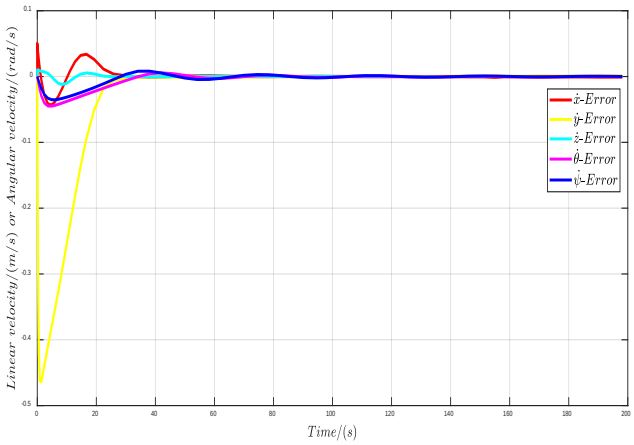

Figure 11. Earth-fixed frame velocity errors of the AUV after 200 *s*

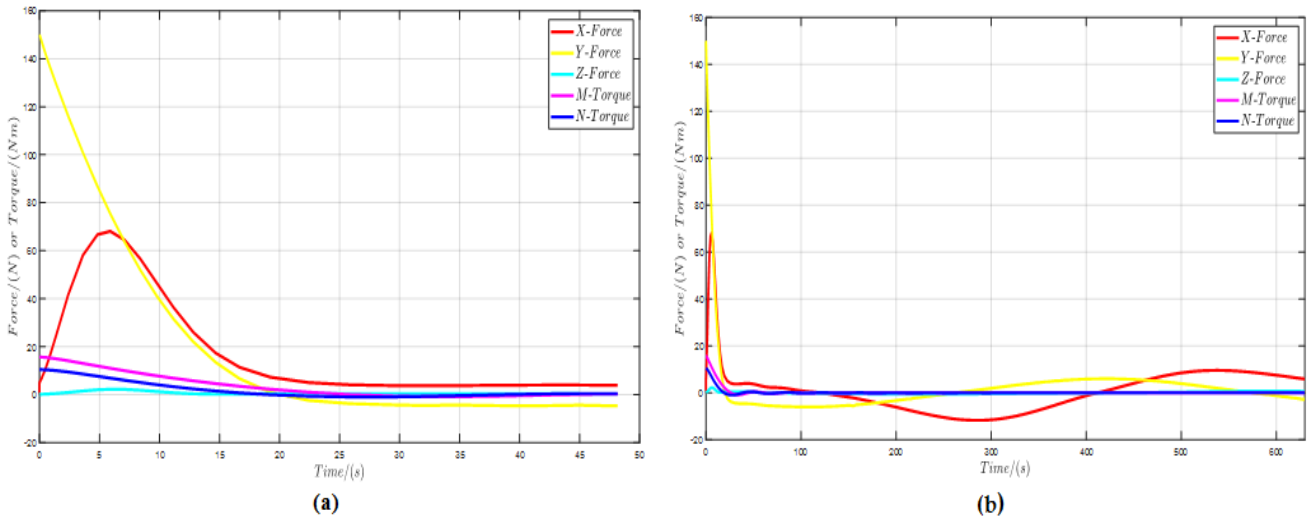

Figure 12. Forces and torques applied to the AUV: (a) after 50 *s*; (b) after 630 *s*

In Figure 12, it is true that initially, both forces and torques have some definite values showing that the AUV accomplished the required acceleration, but after 30 *s*, the torques in case of pitch and yaw converged to zero, which means the angular accelerations became to zero. The forces in case of surge, sway and heave indicate the simple harmonic variation around zero to catch the sinusoidal position inputs, which include the high amplitude in these directions.

5. AUV Path Planning with Optimum Thrust Allocation

5.1. Path Planning Algorithm Using the Adaptive Control Law

In this case, according to the thrust placement given in Figure 1, there are 4 DOFs: surge, roll, pitch, and yaw, in which the AUV is able to maneuver with the controller inputs for the surge u_d, roll $\emptyset_d$, pitch θ_d, and yaw ψ_d DOFs, but the roll DOF behaves like a self-stabilizer. This AUV can move from its current position, called set-point ***A***, to desired potion, called set-point ***B*** as shown in Figure 13.

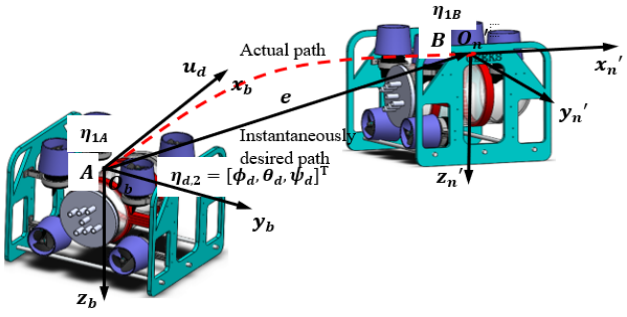

Figure 13. Visualization of the coordinate parameters

The desired point ***B*** is always considered as the origin of the frame that is parallel to the earth fixed frame, while the origin of the body-fixed frame which coincides with the COG is the current position ***A***. The error vector $e(t) = [e_1, e_2, e_3]^T$ describes the position error between the desired point and the current location of the AUV, as shown in Figure 13. The control inputs are provided to steer the AUV along the instantaneously desired path $e(t)$ as the optimum path between ***A*** and ***B*** to minimize the $e(t)$. The AUV is also guided asymptotically towards the desired point ***B***. Note that this control inputs are only valid for $\theta_e \neq \frac{\pi}{2}$, and $\psi_e \neq \frac{\pi}{2}$.

$$e(t) = \eta_{1B} - \eta_{1A} \tag{45}$$

$$u_d = \frac{ke(t)}{\cos(\theta_e)\cos(\psi_e)}; \theta_e = \theta_d - \theta, \psi_e = \psi_d - \psi \tag{46}$$

$$\varnothing_d = 0 \tag{47}$$

$$\theta_d = \tan^{-1}\left(\frac{e_3}{e_1}\right) \tag{48}$$

$$\psi_d = \mathrm{mod}\left(\left(atan2(e_2, e_1) + 2\pi\right), 2\pi\right); 0 \leq \psi_d \leq 2\pi \tag{49}$$

$$\eta_{2,d} = [\varnothing_d, \theta_d, \psi_d]^T. \tag{50}$$

where k is a positive constant.

This control model has the position controller, attitude controller, speed controller and plant (AUV). The desired and current position given in the earth fixed frame are the inputs for the position controller which gives the desired attitude $\eta_{2,d}$, and e as the outputs. The controller discussed in Section 4 is based on the body-fixed frame. Thus, all the inputs for the adaptive controller should be converted to the body-fixed frame. The outputs of the attitude controller are the desired propulsion torques in the roll, pitch, and yaw directions $\tau_{d,4-6}$. Furthermore, e, v, and $\tilde{\eta}_2$ are the inputs for the speed controller giving the propulsion force in the surge direction $\tau_{d,1}$ as the output. The inputs of the plant are $\tau_{d,1}$, $\tau_{d,4-6}$, v, and $\dot{v}$, see Figure 14.

The MATLAB SIMULINK block diagram of this controller is shown in below.

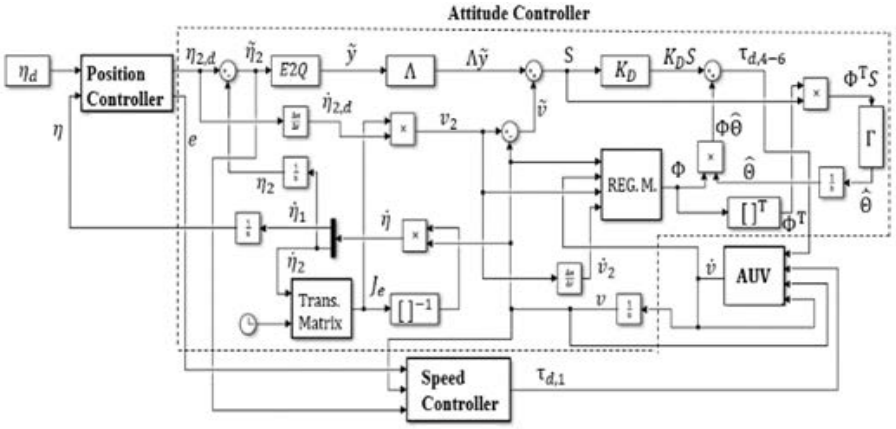

Figure 14. MATLAB SIMULINK layout of the controller

5.2. Optimum Thrust Allocation

In the thrust allocation, optimizing methods are used to minimize the thrust forces to save the power consumption and increase the efficiency of the AUVs. This complex-shaped underwater vehicle contains 6 thrusters and they allow to control the four DOFs: surge, roll, pitch, and yaw. The thruster configuration, thruster forces, thruster numbering and distances are shown with respect to the body-fixed frame in Figure 15.

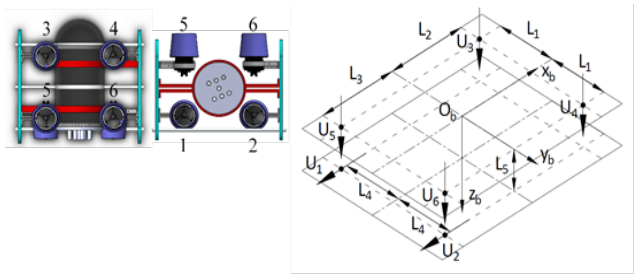

Figure 15. Location of the thrusters on the AUV, definition of the distances, and direction of the positive thrust

The force and torque vector can be defined as follows, seen in [25,31]:

$$\tau = Tf \tag{51}$$

where T is the thruster configuration matrix, indicating the direction of the force in the surge DOF, and the direction of the toques in the roll, pitch, and heave DOFs,

$$T = \begin{bmatrix} 1 & 1 & 0 & 0 & 0 & 0 \\ 0 & 0 & L_1 & -L_1 & L_1 & -L_1 \\ L_5 & L_5 & L_2 & L_2 & -L_3 & -L_3 \\ L_4 & -L_4 & 0 & 0 & 0 & 0 \end{bmatrix} \tag{52}$$

here, the distances L_i are $L_1 = L_4 = 154\ mm$, $L_2 = L_3 = 210\ mm$, and $L_5 = 90\ mm$, and also f is the thrust vector.

$$f = [f_1\ f_2\ f_3\ f_4\ f_5\ f_6]^T \tag{53}$$

The optimum thrust allocation from the required τ can be considered as a model-based optimization problem and it can be categorized under two major categories: constrained thrust allocation and unconstrained thrust allocation. For this AUV, the unconstrained thrust allocation is used because it does not pay an attention about the bounded limitations (minimum and maximum) for the thrust vector. This approach has several advantages than the constrained thrust allocation; it consumes minimum computational time, and requires an on-board computer with low computational power.

Assumption:

The vector of propulsion forces and torques τ is bounded in such a way that the computed elements of the thrust vector f never exceed the boundary values of f_{min} and f_{max}.

Under above assumption, this thrust allocation can be expressed as a problem of the least-squares optimization as follows:

$$\min \frac{1}{2} f^T H f \tag{54}$$

where H is a positive definite matrix.

The solution of (54) using Lagrange multipliers shown in [25] is given by

$$f_{opt} = T^* \tau \tag{55}$$

$$T^* = H^{-1}T^T(TH^{-1}T^T)^{-1} \tag{56}$$

This approach provides a suitable solution for the faultless work of the propulsion system, and cannot be used directly in case of damaged thrusters.

5.2.1. Singular Value Decomposition (SVD) for the Solution

SVD is an eigenvalue-like decomposition for rectangular matrices [32]. After applying the SVD for the thrust configuration matrix, it becomes as follows:

$$T = USV^T \tag{57}$$

where U and V are orthogonal matrices of dimensions 4×4 and $n \times n$, respectively. n is the number of thrusters in the AUV.

$$S = [S_T|\mathrm{O}], S_T = \begin{bmatrix} \gamma_1 & 0 & 0 & 0 \\ 0 & \gamma_2 & 0 & 0 \\ 0 & 0 & \gamma_3 & 0 \\ 0 & 0 & 0 & \gamma_4 \end{bmatrix}. \tag{58}$$

S_T- diagonal matrix of dimensions 4×4
O- null matrix of dimensions $4 \times (n-4)$.

The singular values of T, called $\gamma_1, \gamma_2, \gamma_3$ and γ_4, are positive and the order of them should be like $\gamma_1 \geq \gamma_2 \geq \gamma_3 \geq \gamma_4$. To calculate the optimum thrust vector f_{opt} being a minimum-norm solution to (54), the decomposition form of T is necessary to compute. Finally, f_{opt} can be written in the form of

$$f_{opt} = V \begin{bmatrix} S_T^{-1} \\ \mathrm{O} \end{bmatrix} U^T \tau. \tag{59}$$

5.3. Simulation Results and Discussion

In this section, we present the simulation results of the path planning algorithm and the optimized thrust allocation defined in Section 5.1 and Section 5.2 respectively, including the uncertainty of the hydrodynamic parameters. To simulate the proposed path following algorithm, the AUV requires the earth-fixed frame co-ordinates of the set-point ***A*** and ***B*** for the path planning. It starts form the set-point ***A*** (-8, -8, -2) and is driven through the co-ordinates of the set-point ***B***, see Table 7. All of these points were randomly selected for the simulation. The AUV automatically selects the next set point ***B*** in the sequence given in Table 7. Figure 16 a) and Figure 16 b) show the projection of the path that the AUV followed onto xy and xz plane, respectively. Figure 16 c) presents the path of the AUV in $\mathbb{R}^3$ space.

Table 7. Coordinates of set-point B denoted in the earth-fixed frame

Position of the AUV	Co-ordinates of set-point B					
x_B	-3	2	5	8	5	0
y_B	-2	-5	5	7	2	-1
z_B	0	1	2	0	1	3

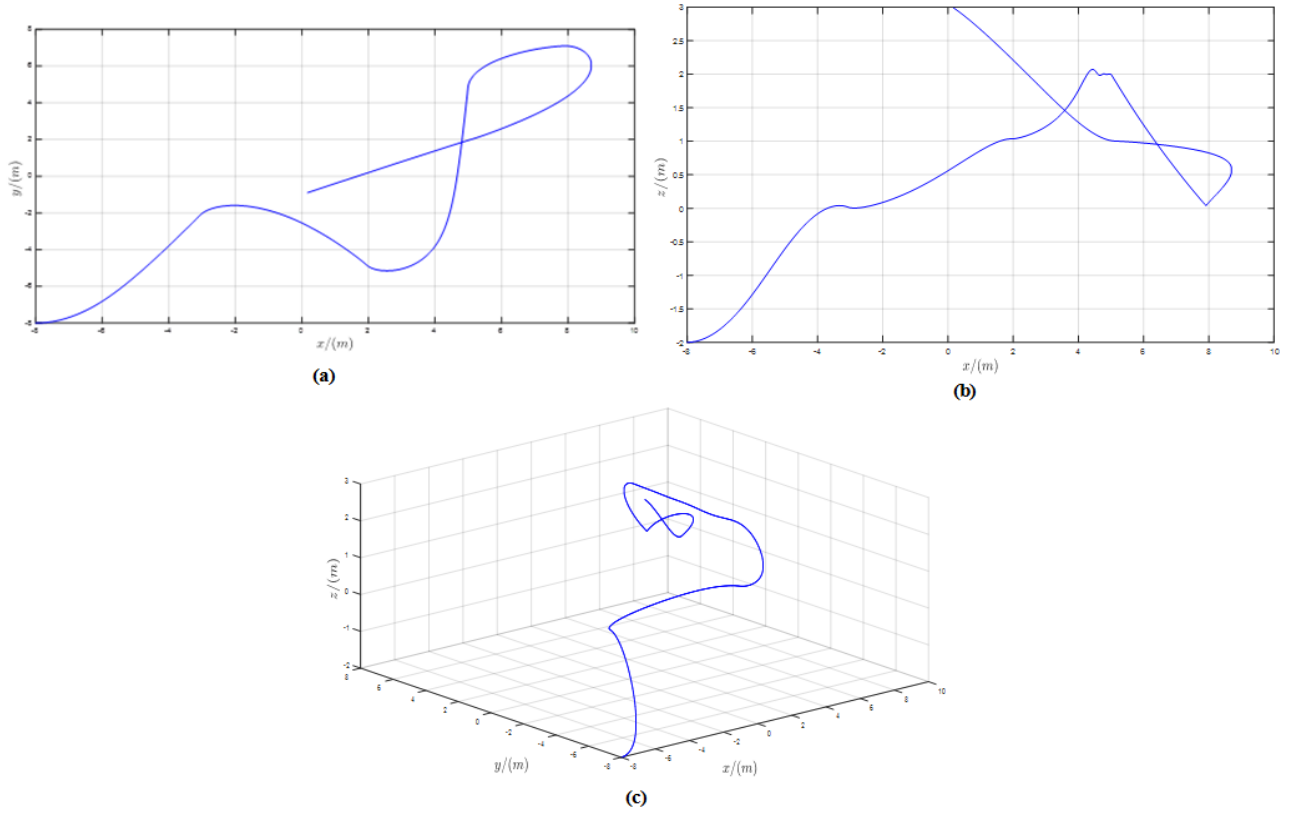

Figure 16. Path of the AUV drawn by its COG: (a) projected onto xy plane; (b) projected onto xz plane; (c) in $\mathbb{R}^3$ space

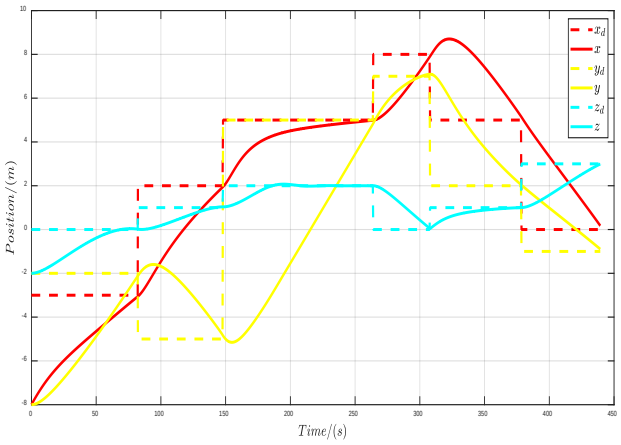

Figure 17. Desired and actual position of the path in the earth-fixed frame

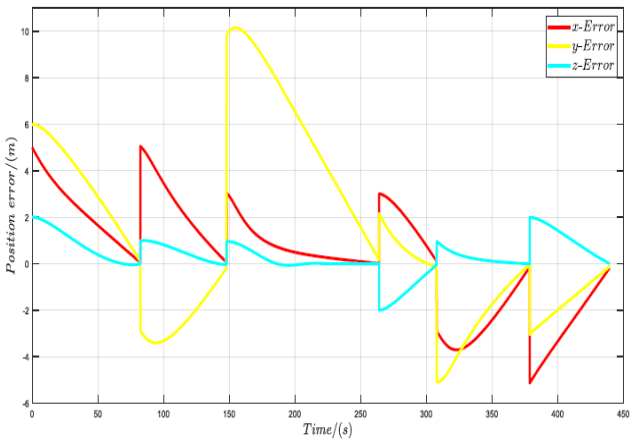

Figure 18. Position error of the path in the earth-fixed frame

The comparison between the desired and actual position is given in Figure 17. The Position error converges to zero at each set-point ***B***, and just after that it increases to match with the new error, as shown in Figure 18.

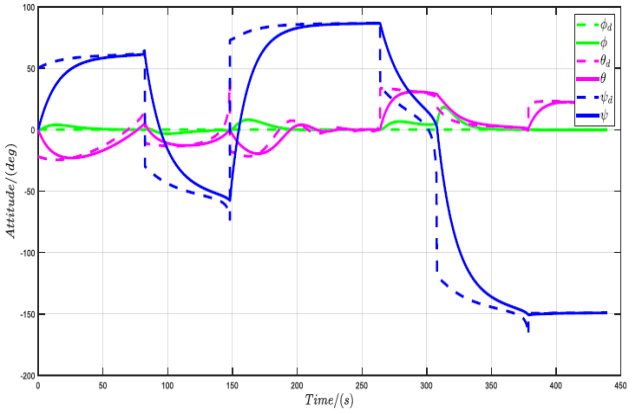

Figure 19. Desired and actual attitude of the path in the earth-fixed frame

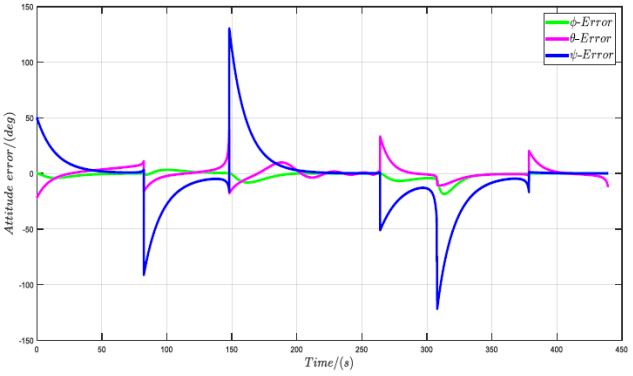

Figure 20. Desired and actual attitude error of the path in the earth-fixed frame

Figure 19 illustrates the desired and actual attitude. In the attitude error given in Figure 20, it is observed that the roll angle always tries to maintain its value around zero like a self-stabilizer. It is important to note that the pitch and yaw angles always vary to match with the optimum path between the current position ***A*** and the set-point ***B***.

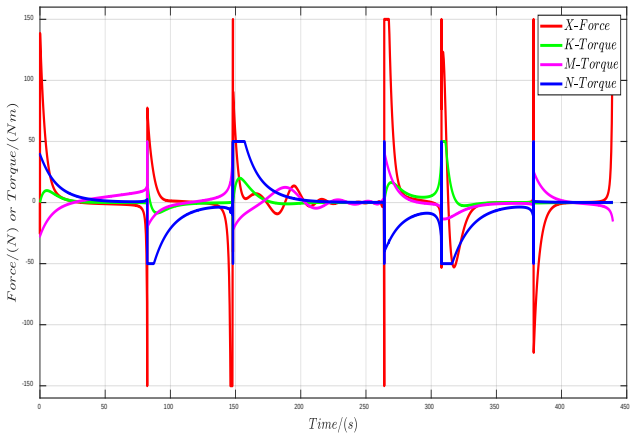

Figure 21. Force and torques applied to the AUV

The Propulsion force in the surge direction and torques in the roll, pitch and yaw directions are indicated in Figure 21. The force and the torques suddenly increase just after reaching each set-point ***B*** since the position and attitude errors instantly grow due to the new target, but they asymptotically converge to zero within $50\,s$, indicating that linear and angular velocities become constant. Thus, we can assume that the AUV runs towards the next set-point ***B*** smoothly.

H, T, U, V, and S_{T} are calculated as below using (57) to compute the optimum thrust allocation for the above discussed AUV;

$$H = \begin{bmatrix} 1 & 0 & 0 & 0 & 0 & 0 \\ 0 & 1 & 0 & 0 & 0 & 0 \\ 0 & 0 & 1 & 0 & 0 & 0 \\ 0 & 0 & 0 & 1 & 0 & 0 \\ 0 & 0 & 0 & 0 & 1 & 0 \\ 0 & 0 & 0 & 0 & 0 & 1 \end{bmatrix} \tag{60}$$

$$T = \begin{bmatrix} 1 & 1 & 0 & 0 & 0 & 0 \\ 0 & 0 & 0.154 & -0.154 & 0.154 & -0.154 \\ 0.090 & 0.090 & 0.210 & 0.210 & -0.210 & -0.210 \\ 0.154 & -0.154 & 0 & 0 & 0 & 0 \end{bmatrix} \tag{61}$$

$$U = \begin{bmatrix} -0.9952 & 0.0981 & 0 & 0 \\ 0 & 0 & 1 & 0 \\ -0.0981 & -0.9952 & 0 & 0 \\ 0 & 0 & 0 & -1 \end{bmatrix} \tag{62}$$

$$V = \begin{bmatrix} -0.7068 & 0.0205 & 0 & -0.7071 & 0 & 0 \\ -0.7068 & 0.0205 & 0 & 0.7071 & 0 & 0 \\ -0.0145 & -0.4998 & 0.5000 & 0 & 0.1000 & 0.7000 \\ -0.0145 & -0.4998 & -0.5000 & 0 & 0.7000 & -0.1000 \\ 0.0145 & 0.4998 & 0.5000 & 0 & 0.7000 & -0.1000 \\ 0.0145 & 0.4998 & -0.5000 & 0 & 0.1000 & 0.7000 \end{bmatrix} \tag{63}$$

$$S_T = \begin{bmatrix} 1.4205 & 0 & 0 & 0 \\ 0 & 0.4181 & 0 & 0 \\ 0 & 0 & 0.3080 & 0 \\ 0 & 0 & 0 & 0.2178 \end{bmatrix}. \tag{64}$$

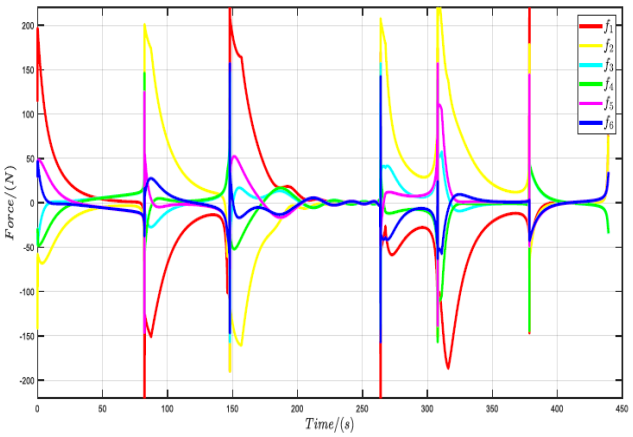

Figure 22. Optimum thrust forces acting on 6 thrusters

The optimum thrust forces f_{opt} derived in (59) are shown in Figure 22. This figure indicates the variation of the thrust vector under the assumption of the unconstrained thrust allocation as discussed in Section 5.2. Generally, $f1$ and $f2$ are much higher than the others

since they provide the propulsion force in the surge direction. Particularly, at the beginning of each new set-point ***B***, all the thrusters show their peak thrust forces. And also, each pair of the thrusters acts in the opposite direction to create the moments for at least one attitude.

6. Conclusion

By avoiding the expensive devices, this paper presents the numerical solution to find the hydrodynamic parameters and it showed that the damping is varied in the quadratic form leading the non-linearity in the AUV model, which should be carefully considered when any linear based controller is designed. Furthermore, an adaptive control law is proposed to track the trajectories, including the uncertainty of the hydrodynamic parameters and using quaternion-based attitude error. Lyapunov's direct approach is used to verify the stability of the proposed control law. It is also developed to plan the optimum path through the given co-ordinates using the concept of the convergence of geometric errors. Finally, an algorithm based on the decomposition of the thrust configuration matrix is used to optimize the unconstrained thrust allocation for the given six thrusters' configuration. The accuracy of the developed control law is verified by the results of the numerical simulation.

Appendix A

By defining the mutual orientation between two frames of common origin of the rotation matrix.

$$R_n(\delta) = I_3 + sin(\delta)\,\hat{n} + (1 - cos(\delta))\hat{n}^2 \qquad (65)$$

where δ is the angle and $n\,\epsilon\,\mathbb{R}^3$ is the unit vector of the axis expressing the rotation needed to align the two frames. $\hat{p}$ is the matrix operator performing the cross product between two (3×1) vectors.

$$\hat{p} = \begin{bmatrix} 0 & -p_3 & p_2 \\ p_3 & 0 & -p_1 \\ -p_2 & p_1 & 0 \end{bmatrix} \qquad (66)$$

The unit quaternion is

$$Q = \{\varepsilon, \mu\} \qquad (67)$$

with

$$\varepsilon = nsin\left(\frac{\delta}{2}\right), \mu = \cos\left(\frac{\delta}{2}\right) \qquad (68)$$

where $\mu \geq 0$ for $\varepsilon = [-\pi, \pi]\ rad.$

The unit quaternion satisfies the condition

$$\mu^2 + \varepsilon\varepsilon^{\mathrm{T}} = 1 \qquad (69)$$

Let's define the vector $\eta_q \boldsymbol{\epsilon} \mathbb{R}^7$ as follows:

$$\eta_q = \begin{bmatrix} \eta_1 \\ Q \end{bmatrix} \qquad (70)$$

The relationship between v and $\dot{\eta}_q$ is given as follows:

$$v = J_q(Q)\dot{\eta}_q \qquad (71)$$

where

$$J_q(Q) = \begin{bmatrix} R_I^B(Q) & 0_{3\times4} \\ 0_{3\times3} & 4J_{k,oq}(Q)^T \end{bmatrix} \qquad (72)$$

$$R_I^B(Q) = \begin{Bmatrix} 1-2\left(\varepsilon_2{}^2 + \varepsilon_3{}^2\right) & 2(\varepsilon_1\varepsilon_2 + \varepsilon_3\mu) & 2(\varepsilon_1\varepsilon_3 - \varepsilon_2\mu) \\ 2(\varepsilon_1\varepsilon_2 - \varepsilon_3\mu) & 1-2\left(\varepsilon_1{}^2 + \varepsilon_3{}^2\right) & 2(\varepsilon_2\varepsilon_3 + \varepsilon_1\mu) \\ 2(\varepsilon_1\varepsilon_3 + \varepsilon_2\mu) & 2(\varepsilon_2\varepsilon_3 - \varepsilon_1\mu) & 1-2\left(\varepsilon_1{}^2 + \varepsilon_2{}^2\right) \end{Bmatrix} \qquad (73)$$

and

$$J_{k,oq}(Q) = \begin{bmatrix} \mu & -\varepsilon_3 & \varepsilon_2 \\ \varepsilon_3 & \mu & -\varepsilon_1 \\ -\varepsilon_2 & \varepsilon_1 & \mu \\ -\varepsilon_1 & -\varepsilon_2 & -\varepsilon_3 \end{bmatrix},\ J_{k,oq}{}^T J_{k,oq} = \frac{1}{4} I_3 \qquad (74)$$

References

[1] I. Yamamoto, "Robust and non-linear control of marine system," *International Journal of Robust and Nonlinear Control*, 11 (13), 1285-1341, Aug.2001.

[2] B. M. Ferreira, A. C. Matos, and N. A. Cruz, "Modeling and control of trimares auv," in *12th International Conference on Autonomous Robot Systems and Competitions*, Portugal, 57-62 April 2012.

[3] Berge S. and Fossen T.I., "Robust control allocation of over actuated ships: Experiments with a model ship," in *4th IFAC Conference on Manoeuvring and Control of Marine Craft*, Brijuni, Croatia, 161-171.

[4] M. Caccia, G. Indiveri, and G. Veruggio, "Modeling and identification of open-frame variable configuration unmanned underwater vehicles," *IEEE Journal of Oceanic Engineering*, 25 (2), 227-240, 2000.

[5] M. E. Rentschler, F. S. Hover, and C. Chryssostomidis, "Modeling and control of an odyssey iii auv through system identification tests," in *Conference on Unmanned Untethered Submersible Technology*, Durham, USA, Aug.2003.

[6] B. Ferreira, M. Pinto, A. Matos, and N. Cruz, "Hydrodynamic modeling and motion limits of auv mares," in *35th Annual Conference of IEEE on Industrial Electronics*, Proto, 2241-2246.

[7] Y.H. Eng, M.W. Lau, and C.S. Chin, "Added mass computation for control of an open-frame remotely-operated vehicle: Application using WAMIT and MATLAB," *Marine Science and Technology*, 22 (2). 1-14, 2013.

[8] Y. H. Eng, W. S. Lau, E. Low, and G. G. L. Seet, " Identification of the hydrodynamics coefficients of an underwater vehicle using free decay pendulum motion," in *International Multiconference of Engineers and Computer Scientists*, Hong Kong, Vol.2, 423-430, March 2008.

[9] L. Wang, H. M. Jia, L. J. Zhang, H. B. Wang., "Horizontal tracking control for AUV based on nonlinear sliding mode," in *IEEE International Conference on Information and Automation (ICIA)*, IEEE, Shenyang, China, 460-463, 2012.

[10] F. Repoulias, E. Papadopoulos, "Planar trajectory planning and tracking control design for underactuated AUVs," *Ocean Engineering*, 34 (11), 1650-1667, 2007.

[11] W. Caharija, K. Y. Pettersen, J. T. Gravdahl, E. Borhaug, "Path following of underactuated autonomous underwater vehicles in the presence of ocean currents," in *51st IEEE Conference on Decision and Control (CDC)*, IEEE, Maui, HI, USA, 528-535, 2012.

[12] F. D. Gao, C. Y. Pan, Y. Y. Han, X. Zhang, "Nonlinear trajectory tracking control of a new autonomous underwater vehicle in complex sea conditions," *Journal of Central South University*, 19 (7), 1859-1868, 2012.

[13] R. N. Smith, Y. Chao, P. P. Li, D. A. Caron, B. H. Jones, G. S. Sukhatme, "Planning and implementing trajectories for autonomous underwater vehicles to track evolving ocean processes based on predictions from a regional ocean model," *International Journal of Robotics Research*, 29 (12). 1475-1479, 2010.

[14] D. Chwa, "Fuzzy adaptive tracking control of wheeled mobile robots with state-dependent kinematic and dynamic disturbances," *IEEE Transactions on Fuzzy Systems*, 20 (3). 587-593, 2012.

[15] X. Q. Bian, J. J. Zhou, Z. P. Yan, H. N. Jia, "Adaptive neural network control system of path following for AUVs," in *Proceedings of the Southeastcon*, IEEE, Orlando, FL, USA, 1-5, 2012.

[16] B. B. Miao, T. S. Li, W. L. Luo, "A DSC and MLP based robust adaptive NN tracking control for underwater vehicle," *Neurocomputing*, 111, 184-189, 2013.

[17] O. Mohareri, R. Dhaouadi, A. B. Rad, "Indirect adaptive tracking control of a nonholonomic mobile robot via neural networks," *Neurocomputing*, 88, 54-66, 2012.

[18] B. Garau, M. Bonet, A. ´Alvarez, S. Ruiz, A. Pascual, "Path planning for autonomous underwater vehicles in realistic oceanic current fields: Application to gliders in the western Mediterranean Sea," *Journal of Maritime Research*, 6 (2), 5-21, 2009.

[19] D. Kruger, R. Stolkin, A. Blum, J. Briganti, "Optimal AUV path planning for extended missions in complex, fast-flowing estuarine environments," in *IEEE International Conference on Robotics and Automation*, IEEE, Roma, Italy, 4265-4270, 2007.

[20] J. Ghommam, O. Calvo, A. Rozenfeld, "Coordinated path following for multiple underactuated AUVs," in *International Conference of OCEANS MTS/IEEE Kobe Techno-Ocean*, IEEE, Kobe, Japan, 1-7, 2008.

[21] H. Bo, R. Hongge, Y. Ke, H. Luyue, R. Chunyun, "Path planning and tracking for autonomous underwater vehicles," in *IEEE International Conference on Information and Automation*, IEEE, Zhuhai/Macau, China, 728-733, 2009.

[22] X. B. Xiang, L. Lapierre, C. Liu, B. Jouvencel. "Path tracking: Combined path following and trajectory tracking for autonomous underwater vehicles," in *IEEE/RSJ International Conference on Intelligent Robots and Systems*, IEEE, San Francisco, USA, 3558-3563, 2011.

[23] GrabCAD community. Available: https://grabcad.com/library/rov-54 (accessed on 20 April 2019).

[24] Thor I. Fossen, Marine control systems: guidance, navigation and control of ships, rigs and underwater vehicles, Marine Cybernetics Trondheim, Norwasy, 2002.

[25] Thor I. Fossen, Guidance and Control of Ocean Vehicles, Wiley, New York, 1994.

[26] SNAME, Nomenclature for treating the motion of a submerged body through a fluid, The Society of Naval Architects and Marine Engineers, New York, 1950.

[27] W. Wang and C. M. Clark, Modeling and Simulation of the Video Ray Pro III Underwater Vehicle, University of Waterloo, Canada, 2001.

[28] D. Perrault, N. Bose, S. O'Young, and C. D. Williams, "Sensitivity of auv added mass coefficients to variations in hull and control plane geometry," *Ocean engineering*, 30 (5), 645-671, 2003.

[29] J. J. E. Slotine, W. Li, Applied Nonlinear Control, Englewood Cliffs, NJ: Prentice-Hall, 1991.

[30] A. C. Huang, M. C. Chien, Adaptive Control of Robot Manipulators: A Unified Regressor-free Approach, Singapore: World Scientific Publishing Company, 2010.

[31] J.Garus, " Fault tolerant control of remotely operated vehicle," in *9th IEEE Conference on Methods and Models in Automation and Robotics*, Miedzyzdroje, Poland, 217-221.

[32] A. Kiełbasinski and K. Schwetlich, Numerical Linear Algebra, Warsaw: WNT, 1992.